J Mol Model (2013) 19:1875–1881
DOI 10.1007/s00894-012-1748-x

ORIGINAL PAPER

First-principles study of ammonium ions and their hydration in montmorillonites

Jing Shi · Houbin Liu · Yingfeng Meng · Zhaoyang Lou · Qun Zeng · Mingli Yang

Received: 21 November 2012 / Accepted: 21 December 2012 / Published online: 17 January 2013

Abstract Density functional theory calculations were performed to investigate the adsorption and hydration of an ammonium ion (NH_4^+) confined in the interlayer space of montmorillonites (MMT). NH_4^+ is trapped in the six-oxygen-ring on the internal surface and forms a strong binding with the surface O atoms. The hydration of NH_4^+ is affected significantly by the surface. Water molecules prefer the surface sites, and do not bind with the NH_4^+ unless enough water molecules are supplied. Moreover, the water molecules involved in NH_4^+ hydration tend to bind with the surface simultaneously. The hydration energy increases with the intercalated water molecules, in contrast to that in gas phase. In addition, the hydration leads to the extension of MMT basal spacing.

Keywords Adsorption · Ammonium ions · Density functional theory · Hydration · Montmorillonite

Introduction

Montmorillonites (MMT) are characterized by their laminar structures consisting of alternative octahedral aluminas and tetrahedral silicas. In a typical MMT structure, isomorphic substitutions of low-valence cations in the silica or the alumina sheet leave extra negative charge in the layer. In order to balance the negative charge, counterions including Na^+, K^+, NH_4^+, Mg^{2+}, Ca^{2+}, Fe^{3+}, etc. intercalate into the interlayer space, resulting in various specific properties like cation exchange, swelling, nano-sheets, etc. [1–10]. The study of NH_4^+ intercalation has particular importance in petroleum engineering, environment protection, and material research. Ammonium ions are one of the main components of drilling fluid, effective in filtration reduction, swelling inhibition, and well-bore stabilization [11–13]. Ammonium ions also exist in waste water, depositing beneath stratum together with other wastes [11, 14–16]. Since MMT layers are about 1 nm in width, they are natural additives in the preparation of nano-composites [17–23]. Ammonium ions and their hydration are often used to split MMT into separate sheets in nano size. In all these processes, the NH_4^+-MMT interaction plays a key role and has attracted much interest in past years. X-ray diffraction (XRD), infrared (IR) spectrum, and scanning electron microscope (SEM) techniques have been employed to investigate the structures of ammonium-clay systems, confirming that NH_4^+ and its hydrates are confined in the interlayer space and interact with the internal surface [24–30]. To our knowledge, however, neither the adsorption nor the hydration of NH_4^+ on the internal surface of clays has been theoretically studied although first-principles calculations have been proven an effective way in the study of molecular adsorption on surfaces [31–35]. In this work, we study the structures of NH_4^+ and its hydrates inside MMT, as well as their interaction with the atoms on the internal surfaces by means of density functional theory (DFT) calculations. Our calculations aim to reveal how an NH_4^+ ion adsorbs on MMT surface, how water molecules affect the NH_4^+ adsorption, and how the adsorption affects MMT structures, all of which are interesting for understanding ammonium ions' diffusion, deposition, transportation, and activity inside MMT.

J. Shi · H. Liu · Y. Meng (✉)
State Key Laboratory of Oil and Gas Reservoir Geology and Exploration, School of Petroleum Engineering, Southwest Petroleum University, Chengdu 610500, China
e-mail: cwctmyf@swpu.edu.cn

Z. Lou · Q. Zeng · M. Yang (✉)
Institute of Atomic and Molecular Physics, Sichuan University, Chengdu 610065, China
e-mail: myang@scu.edu.cn

Methodology

Several structural models have been reported so far for Li-, Na-, K-, Cs- and Ca-MMT [36–40]. In this work, the initial atomic coordinates of MMT was taken from the measurement of Na- and Ca-MMT by Viani [39] with XRD. In this model, no isomorphic substitution was imposed. To obtain negatively charged layers, the structures with Al^{3+}/Mg^{2+} substitution in the alumina layer was constructed. A $2\times1\times1$ supercell with one Al^{3+}/Mg^{2+} isomorphic substitution was used in the calculations. Figure 1 displays the laminar structure of MMT in which two internal surfaces are opposite and form a basal spacing for the encapsulation of counterions and other guest molecules. NH_4^+ and H_2O were placed randomly in the space, followed by a Monte-Carlo (MC) simulation with CLAYFF force field [41] to locate their optimal adsorption sites. The CLAYFF parameters have been found feasible for clay systems [42–45]. At least two independent MC runs for each configuration were carried out and three or more MC-predicted structures along with some additional structures designed from chemical intuition for each system were collected for further studies at DFT level.

All the DFT calculations were carried out under the generalized gradient approximation (GGA) of Perdew-Burke-Ernzerhof (PBE) parameterization [46], as implemented in the SIESTA program [47, 48]. The non-local norm-conserving pseudopotentials in the Troullier-Martins form [49] were used to describe the core electrons, while the valence wave functions are expanded on (pseudo) atomic orbitals including multiple-ζ and polarization functions. The standard DZP basis set with orbital-confining cutoff radii of 0.02 Ry and a real-space integration grid with a plane wave cutoff of 220 Ry were used in this work. Calculations were restricted to the Γ-point in the Brillouin zone [50, 51]. As hydrogen bonds (HBs) are formed among NH_4^+, H_2O and the surface, a dispersion potential of the Grimme type [52] was used to deal with the weak interaction in the systems. The optimal basal spacing of each system was determined by optimizing all the atomic positions at a series of spacings. The conjugated gradient approach was used in the geometry relaxation and the convergence criterion was set to 0.01 eV $Å^{-1}$ in atomic force.

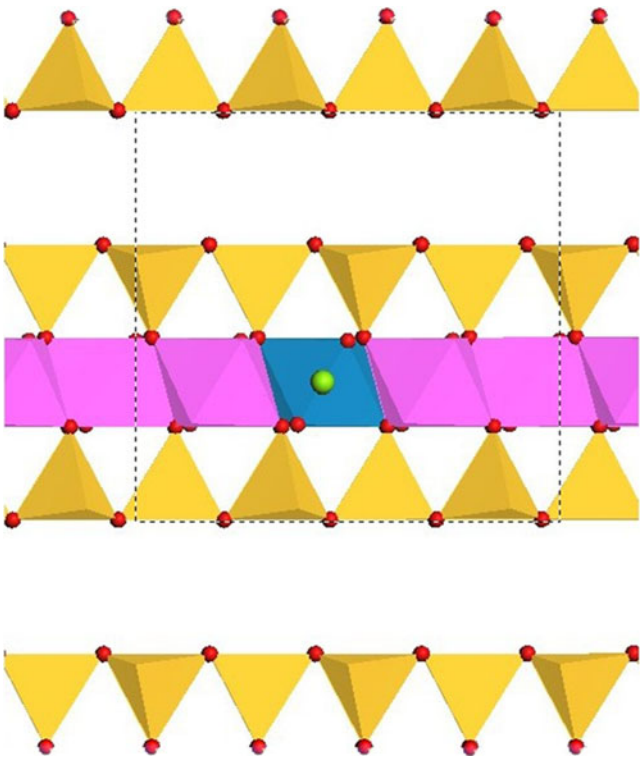

Fig. 1 The laminar structure of MMT. The tetrahedral silica sheet is in yellow and the octahedral alumina sheet in pink except the blue one in which the Al^{3+} is replaced by Mg^{2+} (*green ball*)

Results and discussion

Viani's model gives only a general atomic arrangement in MMT, whereas the MMT structures vary with the in-layer isomorphic substitution (Si^{4+}/Al^{3+} and/or Al^{3+}/Mg^{2+}), counterion (charge and ionic radius) intercalation, and ionic hydration, etc. We first compared the MMT structures with and without Al^{3+}/Mg^{2+} substitution in the alumina layer in the absence of counterion or water in the interlayer space. Figure 2 displays their energy variation with the width of basal space, which is the distance between adjacent layers. In the cubic MMT cell, the basal spacing is just the cell parameter along the *c*-axis. A small width extension of 0.01 Å is noted for the Al^{3+}/Mg^{2+} substitution. Since the substitution leaves an extra negative charge, the internal surfaces become more negative, resulting in stronger electrostatic repulsion between two opposite surfaces. In our calculations, the substitution brings the surface 0.06 e more negative charge, which was obtained by summing up the net charge on all the surface atoms from Mulliken analysis. Since the substitution occurs in the middle alumina layer, such effect is

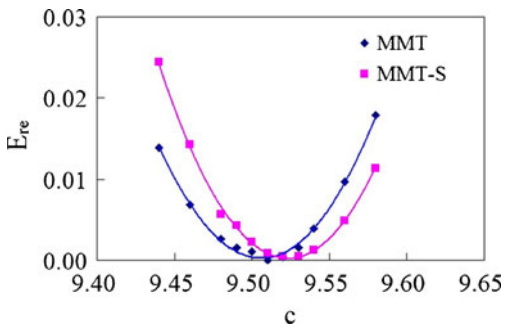

Fig. 2 Energy variations (in eV) of non-substituted (*diamonds*) and Al^{3+}/Mg^{2+} substituted (*squares*) MMT with the basal spacing *c* (in Å). A small increase of *c* is noted upon Al^{3+}/Mg^{2+} substitution

rather small. Only the MMT structures with Al^{3+}/Mg^{2+} substitution were studied below. Because of the narrow interlayer space, the guest ions or molecules may interact with both the upper and the lower surfaces simultaneously.

Next, we look at the atomic arrangement on the internal surface, which is covered by O atoms of silicas. Every six O atoms and six Si atoms constitute a cyclic structure in which the O atoms form a six-O-ring (SOR) on the surface. The SOR is a cation trapper with net negative charge. Precisely, three of the six O atoms protrude outward a little more than the other three, having greater tendency to bind with the counterions.

Screened from a number of candidate structures, only two conformers of NH_4^+ adsorption were identified at DFT level, as presented in Fig. 3, namely W0A and W0B, where Wx denotes the number of water molecules and the last character orders the relative stability. The imagined conformation, two H atoms of NH_4^+ binding with two surface O atoms, is unstable and changes into either W0A or W0B after geometry optimization. In both structures, NH_4^+ is trapped by the SOR with one of its H atoms sunk into the surface and forming three hydrogen bonds (HB) with the surface O atoms, while the left four atoms are above the surface. Table 1 lists the computed HB lengths between the adsorbates and between the adsorbates and MMT surface. The HB lengths are about 1.923 Å for W0A and 2.089 Å for W0B. These two structures are distinguished by the orientation of three outward N-H bonds, which leads to an energy difference of 0.15 eV, as presented in Table 2.

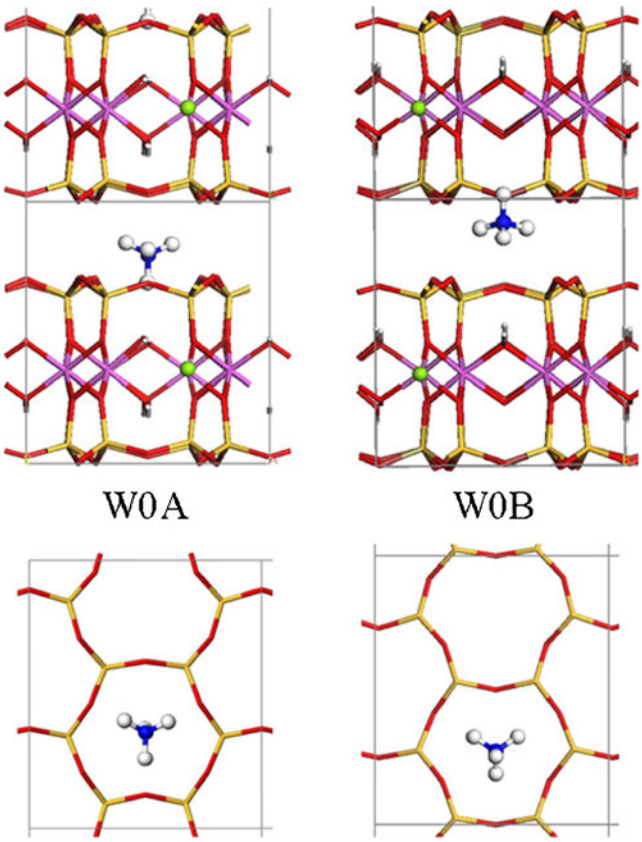

Fig. 3 Side (upper) and top (lower) views of water-free NH_4^+ inside MMT. *Green balls* denote Mg^{2+} ions that replace Al^{3+} in the middle alumina sheet. *Blue* and *gray balls* denote N and H atoms respectively

Table 1 (Averaged) lengths of hydrogen bonds (in Å) between ammonium (A), water (W), and MMT surface (S) atoms in the NH_4^+-$x$$H_2O$-MMT systems. In parentheses are numbers of hydrogen bonds

	R_{A-W}	R_{A-S}	R_{W-W}	R_{W-S}
W0A		1.923 (3)		
W0B		2.089 (3)		
W1A		1.905 (3)		1.715 (2)
W1B		1.905 (3)		1.719 (2)
W1C	1.900 (1)	1.981 (2)		1.810 (2)
W2A	1.887 (1)	1.960 (2)		1.756 (3)
W2B	1.902 (1)	1.815 (3)	1.552 (1)	1.743 (2)
W2C		1.910 (3)	1.531 (1)	1.837 (3)
W2D	1.699 (2)			1.913 (3)
W3A	1.830 (1)	2.022 (2)	1.569 (1)	1.873 (3)
W3B	1.748 (2)	1.907 (2)	1.929 (2)	1.871 (4)
W4A	1.775 (1)	1.935 (3)	1.623 (3)	1.866 (4)
W4B	1.799 (3)		1.919 (2)	1.965 (6)
W5A	1.697 (2)		1.755 (4)	1.913 (6)
W5B	1.788 (3)		1.843 (3)	1.935 (5)

When one water molecule enters into the interlay space, three kinds of conformers were identified, as presented in Fig. 4. It is interesting to note that the incoming H_2O binds with the surface sites instead of the NH_4^+. It binds solely with either lower (W1A) or upper (W1B) surface via two HBs. W1C is 0.07 eV less stable than W1A, although in W1C H_2O forms one more HB with NH_4^+. It is clear that the stability of NH_4^+-H_2O-MMT systems depends on not only the HB number but also the HB strength. Because the orientation of H_2O is restricted by the directionality of multiple HBs, the HBs are lengthened and weakened in W1C, as presented in Table 1. Our calculations reveal that water molecules prefer the surface sites to the intercalated NH_4^+ if enough space is provided.

The second H_2O generates more possible conformers, among which four types of structures were identified, as shown in Fig. 5. In W2A, one of the two water molecules binds with the surface solely, like the H_2O in W1A. The other one binds with both NH_4^+ and the surface, like the H_2O in W1C. In W2B, one HB is formed between the two water molecules, one of which binds with surface via two HBs and the other binds with both the surface and the NH_4^+. Both H_2O form three HBs in total. W2A and W2B have close energy (ΔE=0.02 eV). W2C is 0.14 eV less stable than W2A. The two water molecules in W2C form an HB between them but do not bind with NH_4^+. In W2D, both H_2O form HBs with the NH_4^+ and the surface, but it is

Table 2 Basal spacings (c, in Å), adsorption energy (E_{ad}, in eV), hydration energy (E_H, in eV), relative energy (E_{re}, in eV) surface charge (Q(S), in a.u.), net charge on NH_4^+ (Q(NH_4), in a.u.) and averaged net charge on water molecules (Q(H_2O), in a.u.) of NH_4^+-$x$$H_2O$-MMT systems

	c	E_{ad}/x	E_H	E_{re}	$Q(S)$	$Q(NH_4)$	$Q(H_2O)$
W0A	9.66	4.27		0.00	−1.03	0.53	
W0B	9.64	4.12		0.15	−1.20	0.63	
W1A	9.76	5.52	1.25	0.00	−1.12	0.51	0.06
W1B	9.76	5.46	1.18	0.06	−1.20	0.48	0.05
W1C	9.90	5.45	1.17	0.07	−1.12	0.51	0.06
W2A	10.03	5.55	1.31	0.00	−1.23	0.50	0.15
W2B	10.33	5.54	1.29	0.02	−1.20	0.47	0.12
W2C	10.15	5.48	1.24	0.14	−1.19	0.55	0.14
W2D	10.14	5.33	0.94	0.43	−1.16	0.42	0.13
W3A	10.33	5.65	1.57	0.00	−1.26	0.47	0.13
W3B	11.02	5.62	1.49	0.08	−1.21	0.39	0.09
W4A	10.75	5.70	1.58	0.00	−1.29	0.48	0.07
W4B	11.05	5.68	1.49	0.08	−1.24	0.35	0.09
W5A	11.06	5.76	1.72	0.00	−1.32	0.39	0.06
W5B	11.08	5.75	1.71	0.01	−1.28	0.34	0.08

0.43 eV above W2A. Our calculations reveal that the arrangement of water-water-ammonium (WWA) is energetically favorable on the MMT surface, while the arrangement of water-ammonium-water (WAW), which maximizes the hydration of ammonium ion, is unfavorable on the surface.

With increasing number of water molecules, the candidate pool of possible conformers becomes very large, making the computations extremely demanding. Meanwhile, the structure of water standing solely on the surface becomes unstable because of the narrow interlayer space. While we are interested in the structural variations caused by NH_4^+ adsorption and its hydration, which are mainly related to the number of water molecules, it is reasonable to impose the above rules of water-ammonium arrangement found in NH_4^+-2H_2O-MMT into the construction of candidate structures. Based on such simplifications, we obtained the low-lying structures of NH_4^+-$x$$H_2O$-MMT ($x$=3, 4 and 5), the best two of which are shown in Fig. 6. In W3A, the two H_2O form HBs with each other, all three H_2O form HBs with each other in W3B, while one H_2O in W3A forms an HB with NH_4^+ and two H_2O in W3B form HBs with NH_4^+. Dragged by the water molecules, the H atom of NH_4^+ is no longer below the surface and the NH_4^+ is in fact suspended between two opposite layers. All the adsorbates, water and NH_4^+, form HBs with the surface. The same structural motifs are noted in W4A, W4B, W5A and W5B in which the adsorbates (H_2O and NH_4^+) and MMT surfaces are connected via an HB network. With increasing water number, NH_4^+ forms more HBs with water. Although a water molecule binds first with the surface O atoms, then with other water molecules, the volume effect becomes significant when water number increases, making the water molecules bind with NH_4^+ and with each other. From W1 to W5, the number of ammonium-water (A-W) HBs increases from 0 to 3.

The intercalation of NH_4^+ and water leads to variations in the cell structures and electronic properties. With increasing H_2O, the basal spacing, c, changes from 9.66 Å to 11.08 Å (Table 2), implying that the interlayer space is enlarged by incoming H_2O. Earlier Monte-Carlo simulations [9, 53] pointed out that in Na-MMT, c increases from 9.7 Å to 12.0 Å when the internal surface is covered by one-layer water molecules. As shown in Figs. 3, 4, 5 and 6, the NH_4^+ and water molecules are basically lined up in the middle of interlayer space. However, there remain some vacancies on the surface for additional water molecules. It is expected that the basal spacing could increase further when more water molecules are adsorbed.

The interaction between adsorbates and surface can be evaluated by adsorption energy, which is defined by

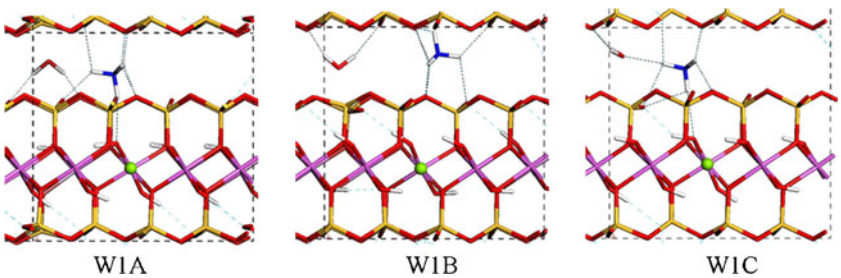

Fig. 4 Side view of the low-lying NH_4^+-1H_2O-MMT structures in which one ammonium ion and one water molecule adsorb on the MMT internal surfaces

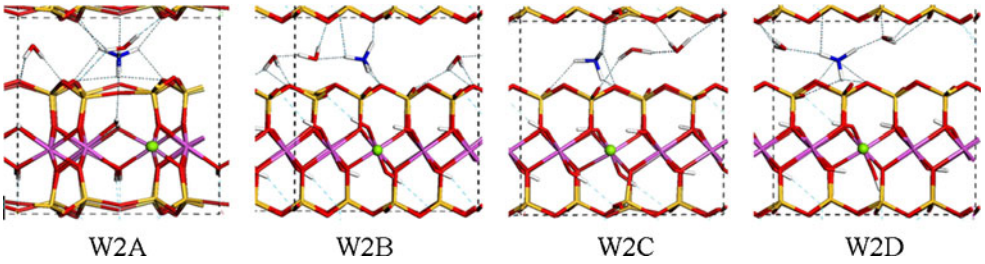

Fig. 5 Side view of the low-lying NH_4^+-$2H_2O$-MMT structures in which one ammonium ion and two water molecules adsorb on the MMT internal surfaces

$$E_{ad} = E(NH_4^+) + xE(H_2O) + E(MMT) - E(NH_4^+\text{-}xH_2O\text{-}MMT) \quad (1)$$

where E(X) is the energy of system X. For an explicit understanding to the hydration effect of the confined NH_4^+, we further define hydration energy as

$$E_H = E\{NH_4^+\text{-}(x-1)H_2O\text{-}MMT\} + E(H_2O) - E(NH_4^+ - xH_2O - MMT) \quad (2)$$

The E_{ad}/x and E_H values are given in Table 2 and Fig. 7. E_{ad}/x has a sharp increase from x=0 to 1, and then has small increases with x, while E_H increases steadily from x=1 to 5. The variation of E_{ad}/x and E_H reflect that with increasing x, more HBs are formed among NH_4^+, H_2O, and MMT surface. The hydration of NH_4^+ in MMT is an energetically favorable process.

The net charge of the adsorbates and the surface is also an indicator of adsorbate-surface interaction. The net charge of NH_4^+, H_2O and MMT are listed in Table 2. In the water-free W0A structure, about 0.53 e electron moves from surface O to NH_4^+. When water enters, NH_4^+ accepts negative charge from water molecules and becomes less positive. Meanwhile, water accepts electrons from the surface.

NH_4^+ in MMT exhibits different hydration behaviors from in gas phase. In a DFT study, Brugé et al. [54] identified the structures of hydrated NH_4^+ and found that four water molecules bind with NH_4^+ one by one via HBs, and the fifth H_2O binds with one of the adsorbed H_2O. These adsorption patterns are not noted among the low-lying structures of hydrated NH_4^+ in MMT because of the strong binding of surface SOR with NH_4^+, as well as the preference of water toward the surface. The BLYP predicted hydration energy in gas is 0.88 eV for first water, and drops to 0.42 eV for the fifth water [54]. In our calculations, the hydration energy increases with the incoming water molecules because of the strong H_2O-surface and NH_4^+-surface interaction. The computed hydration energy is 1.25 eV for the first water and increases to 1.72 eV for the fifth.

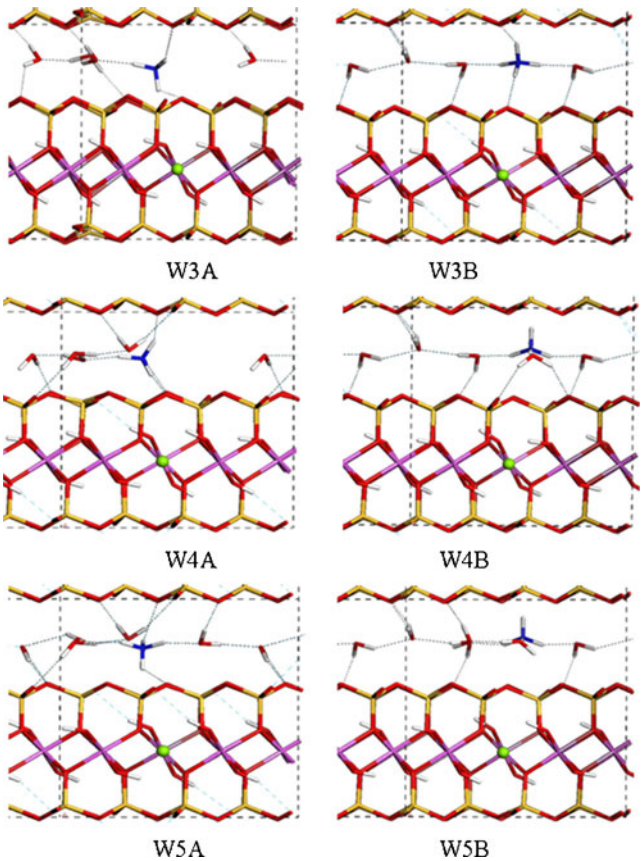

Fig. 6 Side view of the low-lying NH_4^+-xH_2O-MMT (x=3, 4 and 5) structures in which one ammonium ion and x water molecules adsorb on the MMT internal surfaces

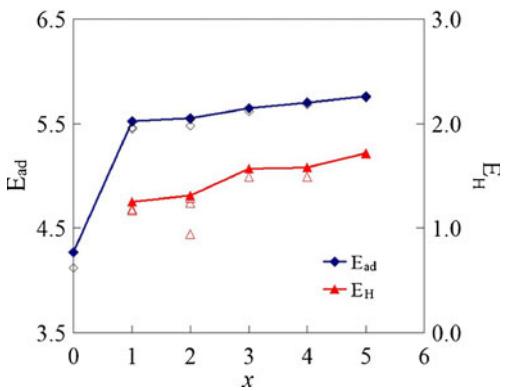

Fig. 7 Variations of adsorption energy (E_{ad}, in eV) and hydration energy (E_H, in eV) with the number of water molecules. The values for the most stable configurations are connected with line

Conclusions

The adsorption and hydration of NH_4^+ in the interlayer space of montmorillonites (MMT) were investigated using periodic density functional theory calculations with the PBE functional plus dispersion correction. The Al^{3+}/Mg^{2+} substitution in the middle alumina layer makes the internal surfaces more negative and favors the intercalation of counterions. NH_4^+ is trapped tightly by the SOR on the surface. In its optimal conformer, one of the H atoms is sunk under the surface, while the other three H atoms stretch outward. Different from the cases in gas phase, water molecules prefer the surface sites to the NH_4^+. With the addition of water molecules, an HB network is gradually formed between water and surface, water and water, water to NH_4^+, and NH_4^+ to surface. All the incoming water molecules bind with the surface via HBs regardless of their interaction with NH_4^+, indicating that the hydration of NH_4^+ in MMT is highly affected by the surface activity. The interaction between the surface and the adsorbates is evaluated in terms of adsorption energy, hydration energy, and the charge transfer among the groups. A strong binding of NH_4^+ with the surface is noted, while water molecules bind weakly with the surface and the NH_4^+. With increasing number of water molecules, the hydration energy increases, accompanied by the increase of basal spacing.

Acknowledgments This work was supported by Open Research Fund of State Key Laboratory of Oil and Gas Reservoir Geology and Exploration (Southwest Petroleum University, No. PLN1118) and National Natural Science Foundation of China (No. 51134004 and 51204142). Part of computations was carried out on the Computer Clusters in Institute of Atomic and Molecular Physics, Sichuan University.

References

1. Boek ES, Coveney PV, Skipper NT (1995) Monte Carlo molecular modeling studies of hydrated Li-, Na-, and K-smectites: understanding the role of potassium as a clay swelling inhibitor. J Am Chem Soc 117:12608–12617
2. Whitley HD, Smith DE (2004) Free energy, energy, and entropy of swelling in Cs-, Na-, and Sr-montmorillonite clays. J Chem Phys 120:5387–5395
3. Tunega D, Haberhauer G, Gerzabek MH, Lischka H (2002) Theoretical study of adsorption sites on the (001) surfaces of 1:1 clay minerals. Langmuir 18:139–147
4. Chatterjee A, Ebina T, Onodera Y, Mizukami F (2004) Effect of exchangeable cation on the swelling property of 2:1 dioctahedral smectite—A periodic first principle study. J Chem Phys 120:3414–3424
5. Liu XD, Lu XC (2006) A Thermodynamic understanding of clay-swelling inhibition by potassium ions. Angew Chem Int Ed 45:6300–6303
6. Tambach TJ, Bolhuis PG, Hensen EJM, Smit B (2006) Hysteresis in clay swelling induced by hydrogen bonding: accurate prediction of swelling states. Langmuir 22:1223–1234
7. Oueslati W, Karmous MS, Rhaiem HB, Lanson B, Amara ABH (2007) Effect of interlayer cation and relative humidity on the hydration properties of a dioctahedral smectite. Z Kristallogr Suppl 26:417–422
8. Morodome S, Kawamura K (2011) In situ X-ray diffraction study of the swelling of montmorillonite as affected by exchangeable cations and temperature. Clays Clay Miner 59:165–175
9. Zeng QH, Yu AB, Lu GQ, Standish RK (2003) Molecular dynamics simulation of organic–inorganic nanocomposites: layering behavior and interlayer structure of organoclays. Chem Mater 15:4732–4738
10. Liu XD, Lu XC, Meijer EJ, Wang RC (2012) Atomic-scale structures of interfaces between phyllosilicate edges and water. Geochim Cosmochim Acta 81:56–68
11. Gautier M, Muller F, Forestier LL, Beny JM, Guegan R (2010) NH_4-smectite: characterization, hydration properties and hydro mechanical behaviour. Appl Clay Sci 49:247–254
12. Mingram B, Bräuer K (2001) Ammonium concentration and nitrogen isotope composition in metasedimentary rocks from different tectonometamorphic units of the European Variscan belt. Geochim Cosmochim Acta 65:273–287
13. Gieskes JM, Mahn C (2007) Halide systematics in interstitial waters of ocean drilling sediment cores. Appl Geochem 22:515–533
14. Christensen TH, Kjeldsen P, Bjerg PL, Jensen DL, Christensen JB, Baun A, Albrechtsen HJ, Heron C (2001) Biogeochemistry of landfill leachate plumes. Appl Geochem 16:659–718
15. Watenphul A, Wunder B, Heinrich W (2009) High-pressure ammonium-bearing silicates: implications for nitrogen and hydrogen storage in the Earth's mantle. Am Mineral 94:283–292
16. Meziti C, Boukerroui A (2011) Regeneration of a solid waste from an edible oil refinery. Ceram Int 37:1953–1957
17. Achilias DS, Siafaka P, Nikolaidis AK (2012) Polymerization kinetics and thermal properties of poly(alkyl methacrylate)/organomodified montmorillonite nanocomposites. Polym Int 61:510–1518
18. Liu N, Wang MX, Liu MM, Liu F, Weng LP, Koopal LK, Tan WF (2012) Sorption of tetracycline on organo-montmorillonites. J Hazard Mater 225:28–35
19. Ma JZ, Deng FQ, Xue CH, Duan ZY (2012) Effect of modification of montmorillonite on the cellular structure and mechanical properties of ethylene vinyl acetate/clay nanocomposite foams. J Reinf Plast Compos 31:1170–1179
20. Mishra AK, Allauddin S, Narayan R, Aminabhavi TM, Raju KVSN (2012) Characterization of surface-modified montmorillonite nanocomposites. Ceram Int 38:929–934
21. Palkova H, Jankovic L, Zimowska M, Madejova J (2011) Alterations of the surface and morphology of tetraalkyl-ammonium modified montmorillonites upon acid treatment. J Colloid Interface Sci 363:213–222
22. Lin KJ, Jeng US, Lin KF (2011) Adsorption and intercalation processes of ionic surfactants on montmorillonite associated with their ionic charge. Mater Chem Phys 131:120–126
23. Tortora M, Gorrasi G, Vittoria V, Galli G, Ritrovati S, Chiellini E (2002) Structural characterization and transport properties of organically modified montmorillonite/polyurethane nanocomposites. Polymer 43:6147–6157
24. Drits VA, Lindgreen H, Salyn AL (1997) Determination of the content and distribution of fixed ammonium in illite-smectite by X-ray diffraction: Application to North Sea illite-smectite. Am Mineral 82:79–87
25. Bobos I, Ghergari L (1999) Conversion of smectite to ammonium illite in the hydrothermal system of Harghita B i, Romania: SEM and TEM investigations. Geol Carpath 50:379–387
26. Jankovic E, Komadel P (2000) Catalytic properties of a heated ammonium-saturated dioctahedral smectite. Collect Czechoslov Chem Commun 65:1527–1536
27. Bishop JL, Banin A, Mancinelli RL, Klovstad MR (2002) Detection of soluble and fixed NH_4^+ in clay minerals by DTA and IR reflectance spectroscopy: a potential tool for planetary surface exploration. Planet Space Sci 50:11–19
28. Pironon J, Pelletier M, de Donato P, Mosser-Ruck R (2003) Characterization of smectite and illite by FTIR spectroscopy of interlayer NH_4^+ cations. Clay Miner 38:201–211

29. Drits VA, Sakharov BA, Salyn AL, Lindgreen H (2005) Determination of the content and distribution of fixed ammonium in illite-smectite using a modified X-ray diffraction technique: application to oil source rocks of western Greenland. Am Mineral 90:71–84
30. Torsten S, Christian K (2009) Structural characterization of (Cu^{2+}, Na^{+})- and (Cu^{2+}, NH_4^{+})- exchanged bentonites upon thermal treatment. Clays Clay Miner 57:40–45
31. Shalabi AS, Assem MM, Soliman KA (2011) Adsorption and spin state properties of Cr, Ni, Mo, and Pt deposited on Li^{+} and Na^{+} monovalent cation impurities of MgO (001) surface: DFT calculations. J Mol Model 17:3299–3308
32. Boulet P, Knofel C, Kuchta B, Hornebecq V, Llewellyn PL (2012) Computational investigation of the adsorption of carbon dioxide onto zirconium oxide clusters. J Mol Model 18:4819–4830
33. Blowers P, Kim BG (2011) The adsorption of mercury-species on relaxed and rumpled CaO (0 0 1) surfaces investigated by density functional theory. J Mol Model 17:505–514
34. Lou ZY, Zeng Q, Chu X, Yang F, Yang ML, Xiang ML, Zhang XD, Fan HS (2012) First-principles study of the adsorption of lysine on hydroxyapatite (1 0 0) surface. Appl Surf Sci 258:4911–4916
35. Shi J, Liu HB, Lou ZY, Zhang Y, Meng YF, Zeng Q, Yang ML (2013) Effect of interlayer counterions on the structures of dry montmorillonites with Si^{4+}/Al^{3+} substitution. Comput Mater 69:95–99
36. Zvyagin BB, Pinsker ZG (1949) Electron diffraction study of the montmorillonite structure. Dokl Acad Nauk SSSR 68:30–35
37. Tsipursky SI, Drits VD (1984) The distribution of octahedral cations in the 2:1 layers of dioctahedral smectites studied by oblique-texture electron diffraction. Clay Miner 19:177–193
38. Skipper NT, Chang FRC, Sposito G (1995) Monte Carlo simulation of interlayer molecular structure in swelling clay minerals. 1. Methodology. Clays Clay Miner 43:285–293
39. Viani A, Gualtieri AF, Artioli G (2002) The nature of disorder in montmorillonite by simulation of X-ray powder patterns. Am Mineral 87:966–975
40. Gournis D, Lappas A, Karakassides MA, Tobbens D, Moukarika A (2008) A neutron diffraction study of alkali cation migration in montmorillonites. Phys Chem Miner 35:49
41. Cygan RT, Liang JJ, Kalinichev AG (2004) Molecular models of hydroxide, oxyhydroxide, and clay phases and the development of a general force field. J Phys Chem B 108:1255–1266
42. Dvoyashkin M, Zang J, Yucelen GI, Katihar A, Nair S, Sholl DS, Bowers CR, Vasenkov S (2012) Diffusion of tetrafluoromethane in single-walled aluminosilicate nanotubes: pulsed field gradient NMR and molecular dynamics simulations. J Chem Phys C 116:21350–21355
43. Zhang GZ, Al-Saidi WA, Myshakin EM, Jordan KD (2012) Dispersion-corrected density functional theory and classical force field calculations of water loading on a pyrophyllite (001) surface. J Chem Phys C 116:17134–17141
44. Ledyastuti M, Liang YF, Kunieda M, Matsuoka T (2012) Asymmetric orientation of toluene molecules at oil-silica interfaces. J Chem Phys 137:064703–064711
45. Tokarsky J, Capkova P, Burda JV (2012) Structure and stability of kaolinite/TiO2 nanocomposite: DFT and MM computations. J Mol Model 18:2689–2698
46. Perdew JP, Burke K, Ernzerhof M (1996) Generalized gradient approximation made simple. Phys Rev Lett 77:3865–3868
47. Sánchez-Portal D, Ordejón P, Artacho E, Soler JM (1997) Density-functional method for very large systems with LCAO basis sets. Int J Quantum Chem 65:453–461
48. Soler JM, Artacho E, Gale JD, García A, Junquera J, Ordejón P, Sáanchez-Portal D (2002) The Siesta method for *ab initio* order-N materials simulation. J Phys Condense Matter 14:2745–2779
49. Troullier N, Martins JL (1991) Efficient pseudopotentials for plane-wave calculations. Phys Rev B 43:1993–2006
50. Sainz-Díaz CI, Timón V, Botella V, Artacho E, Hernández-Laguna A (2002) Quantum mechanical calculations of dioctahedral 2:1 phyllosilicates: Effect of octahedral cation distributions in pyrophyllite, illite, and smectite. Am Mineral 87:958–965
51. Stich I, Parrinello M, Holender JM (1996) Dynamics, spin fluctuations, and bonding in liquid silicon. Phys Rev Lett 76:2077–2080
52. Grimme S (2006) Semiempirical GGA-type density functional constructed with a long-range dispersion correction. J Comput Chem 27:1787–1799
53. Karaborni S, Smit B, Heidug W, Urai J, Oort EV (1996) The swelling of clays: molecular simulations of the hydration of montmorillonite. Science 271:1102–1104
54. Brugé F, Bernasconi M, Parrinello M (1999) Density-functional study of hydration of ammonium in water clusters. J Chem Phys 110:4734–4736